DMD Fast Forward. Published on September 10, 2014 as DOI: 10.1124/dmd.114.060319
This article has not been copyedited and formatted. The final version may differ from this version.

Evaluation of Near IR Fluorescent Labeling of mAbs as a Tool for Tissue Distribution

Kip P. Conner, Brooke M. Rock, Gayle K. Kwon, Joseph P. Balthasar, Lubna Abaquayyas, Larry C. Wienkers and Dan A. Rock

Biochemistry and Biophysics Group in Pharmacokinetics and Drug Metabolism, Amgen Inc. Seattle, WA (KPC, BMR, GKK, LCW, DAR)

Department of Pharmaceutical Sciences, University at Buffalo, The State University of New York, Buffalo, NY (JPB)

Quantitative Pharmacology Group in Pharmacokinetics and Drug Metabolism, Amgen Inc. Thousand Oaks, CA (LA)

Running Title Page

Running Title: Near IR Labeling for Tissue Distribution

Address for Correspondence:

Dan A Rock

1201 Amgen Court West

Seattle, WA 98119

Ph: (206) 265-7139

Fax: (206) 265-1149

E-mail: drock@amgen.com

Text pages: 25

Tables: 2

Figures: 5

References: 25

Abstract (250 words): 250

Introduction (750 words): 770

Discussion words (1500 words): 1,528

Abbreviations: Area under the curve (AUC), Enzyme linked immunosorbent assay (ELISA), Fragment crystallizable domain (Fc), IRDye800® (IR800), Neonatal Fc receptor (FcRn), Near infrared (NIR), Monoclonal antibody (mAb), Mouse monoclonal IgG1 (8C2), Pharmacokinetic (PK), Target-mediated drug disposition (TMDD), Degree of labeling (DOL), Region of Interest (ROI), Size exclusion chromatography (SEC)

DMD Fast Forward. Published on September 10, 2014 as DOI: 10.1124/dmd.114.060319
This article has not been copyedited and formatted. The final version may differ from this version.

Abstract

The pharmacokinetic (PK) behavior of monoclonal antibodies (mAbs) is influenced by target-mediated drug disposition (TMDD), off-target effects, anti-drug antibody mediated clearance, and interaction with Fc receptors such as FcRn. All of these interactions hold the potential to impact mAb biodistribution. Near-infrared (NIR) fluorescent probes offer a complementary approach to radionuclides to characterize drug disposition. Notably, the use of FDA-approved IRDye800® (IR800; LI-COR®) as a protein labeling agent in preclinical work holds the potential for quantitative tissue analysis. Here, we tested the utility of the IR800 dye as a quantitative mAb tracer during pharmacokinetic analysis in both plasma and tissues using a model mouse monoclonal IgG1 (8C2) labeled with ≤ 1.5 molecules of IR800. The plasma PK parameters derived from a mixture of IR800-8C2 and 8C2 dosed intravenously to C57BL/6 mice at 8 mg/kg exhibited a large discrepancy in exposure dependent on the method of quantitation (CL_{plasma} = 8.4 mL/day/kg (NIR fluorescence detection) versus 2.5 mL/day/kg (ELISA)). The disagreement between measurements suggests that the PK of 8C2 is altered by addition of the IR800 dye. Additionally, direct fluorescence analysis of homogenized tissues revealed several large differences in IR800-8C2 tissue uptake when compared with a previously published study using ^{125}I-8C2 (Abuqayyas et al., 2012), most notably an over 4-fold increase in liver concentration. Finally, the utility of IR800 in combination with whole body imaging was examined by comparison of IR800-8C2 levels observed in animal saggital cross sections to those measured in homogenized tissues. Our results represent the first PK analysis in both mouse plasma and tissues of an IR800-mAb conjugate and suggest that mAb disposition is significantly altered by IR800 conjugation to 8C2.

Introduction

Monoclonal antibodies (mAbs) embody an attractive therapeutic modality for disease intervention as they combine high affinity and specificity toward their target with biological half-lives conducive to infrequent dosing schedules. In part, the success of mAb therapeutics has sparked efforts to harness the favorable pharmacokinetic properties of the antibody scaffold by fusing the fragment crystallizable domain (Fc) of an IgG with novel biological proteins (Korth-Bradley et al., 2000; Fast et al., 2009; Herzog et al., 2014). However, the absorption, distribution, metabolism and excretion (ADME) of mAb-based proteins are complicated due to interactions with the pharmacological target(s) (e.g. target-mediated drug disposition, or TMDD), the potential influence of anti-drug antibodies, and interactions with Fc receptors. The aforementioned interactions create uncertainty when characterizing the pharmacokinetic and pharmacodynamic responses for mAbs and associated fusion proteins.

Knowledge of the disposition of engineered mAb-based therapeutic proteins that result from complex *in vivo* interactions provides insight into biological activity and/or off-target effects, and can lead to design strategies that maximize the intended therapeutic response. Importantly, if the biodistribution of a candidate therapeutic is sufficiently resolved at the organ level during the design and testing stages of drug discovery, then this information can be useful for defining the parameters that best predict sites of TMDD and/or toxicity.

Radiolabeling of proteins represents an informative technique to study mAb distribution to antigen-specific tissues as well as overall organ exposure. For decades, mAb-based therapuetics have incorporated radionuclide labels for use as diagnostic tools (Sands, 1990; Duncan and Welch, 1993). Different radiolabel tracers possess unique properties upon endogenous processing of the conjugated proteins. Notably, proteins conjugated with ^{111}In and ^{89}Zr exhibit increased mean residence time inside the cell, and as such are coined ‘residualizing’ labels (Duncan and Welch, 1993). Residualizing behavior is believed to arise from a

DMD Fast Forward. Published on September 10, 2014 as DOI: 10.1124/dmd.114.060319
This article has not been copyedited and formatted. The final version may differ from this version.

combination of a slower rate of protein catabolism and elimination from the cell, and is most likely related to intrinsic physical properties of the linker and metal (Geissler et al., 1991; Duncan and Welch, 1993; Zhu et al., 1997; Perera et al., 2007; Lee et al., 2008; Boswell et al., 2010). In contrast, non-residualizing probes that incorporate ^{3}H, ^{14}C, and ^{125}I eliminate their protein and radioisotope catabolites from the cell more rapidly. This subtle distinction *in vivo* for various radioisotopes can be exploited to differentiate mAb tissue accessibility versus catabolic fate (Yip et al., 2014).

Several studies have used radiolabels to identify local off-target expression of an antigen, and to assess the impact of protein engineering on biodistribution and catabolism of mAbs (Aerts et al., 2009; Boswell et al., 2013; Steiner et al., 2013). Although the utility of radiolabels for characterization of therapeutic mAb biodistribution is unquestioned, their use is precluded in many laboratories due to stringent regulatory requirements, in addition to the costly operational overhead. Thus, the availability of a more generally-accessible label would be valuable.

Near infrared (NIR) fluorescent probes combined with optical detection offer a complementary approach to radiolabeling that has gained much interest in the clinical setting (Tanaka et al., 2007; Guo et al., 2014). For detection and imaging, NIR optical probes have several advantages over traditional fluorophores. First, the NIR spectrum is less prone to exciting endogenous fluorophores in animal tissue. Second, the long wavelength excitation and emission spectra of NIR probes allow for enhanced tissue penetration of the applied light source and transmittance of light from the specimen. These probe features result in negligible auto-fluorescence with enhanced signal recovery, and high target-to-background contrast. Last, direct tissue fluorescent measurement has been shown to be quantitative when proper sample dilution is considered (Oliveira et al., 2012). NIR optical probes offer ease of use, are cost effective and require no specialized equipment or added safety precautions.

Numerous options for fluorescent probes and labeling chemistries exist, but the use of indocyanine-based IRDye800® (IR800) from LI-COR® is enticing given its FDA approval, which allows the translation of preclinical data obtained with NIR conjugates to be directly utilized for downstream clinical studies. While characterization of IR800 in tissue has been shown to be quantitative (Oliveira et al., 2012), additional characterization of the PK of IR800-mAb conjugates is warranted. Specifically, preclinical study of IR800-mAb conjugates that do not contain additional radiolabels has yet to be conducted. We sought to compare the *in vivo* behavior of an IR800-mAb to both its unlabeled mAb equivalent, and that bearing the non-residualizing ^{125}I radiolabel. The objective of this current work is to evaluate and compare the pharmacokinetics and biodistribution in mouse of separately labeled IR800 and ^{125}I conjugates of the model murine mAb, 8C2. In addition, the novel combination of whole body sectioning as a tool for imaging biodistribution with IR800 is explored.

DMD Fast Forward. Published on September 10, 2014 as DOI: 10.1124/dmd.114.060319
This article has not been copyedited and formatted. The final version may differ from this version.

Materials and Methods

Materials.

8C2, a murine IgG1 anti-topotecan antibody, was employed as a model mAb for this study. The antibody was produced and purified from the culture of hybridoma cells, as previously described (Chen et al., 2007). Sodium iodide ($Na\cdot^{125}I$) was obtained from Perkin Elmer Inc. (Waltham, MA). Chloramine-T, sodium metabisulfite, calcium sulfate ($CaSO_4$), and carboxymethyl cellulose (CMC) were from Sigma Life Science (St. Louis, MO). Potassium iodide (KI) was obtained from Fisher Scientific (Pittsburgh, PA). IRDye800® (IR800) was purchased from LI-COR® (Lincoln, NE). All other materials were purchased from Sigma-Aldrich (St. Louis, MO), unless specified.

8C2 Labeling.

For conjugation of mAb 8C2 to IR800-NHS, 10 mg of antibody was buffer exchanged into 100 mM potassium phosphate (pH = 8.5) using a Zeba 7kDa MWCO spin-column (Thermo Pierce, Rockfield, IL), prior to dilution to a final reaction concentration of 1.5 mg/mL as determined by UV absorbance (ε_{280nm} = 203,000 M^{-1} cm^{-1} in PBS : MeOH 1:1). A 20 mg/mL (17.2 mM) in DMSO solution of IR800-NHS was then added directly to the protein containing buffer for a final molar excess of activated ester of 3:1. The reaction was shielded from ambient light and allowed to react at room temperature for 2 hours. To quench the reaction of excess activated NHS ester, 100 mM ethanolamine was added as a 1 M stock solution. Free dye and excess ethanolamine was removed from the reaction mixture via multiple rounds of buffer exchange on a Zeba 7kDa MWCO spin column pre-equilibrated in PBS. Size exclusion chromatography was used to verify conjugate purity and the predominance of a monomeric mAb aggregation state monitored by UV/vis detection (215, 280, and 780nm channels). Chromatography was conducted using an 4.6 x 300 mm Bio SEC-3 (30 nm pore, 3µm diameter particle; Agilent) with mobile phase containing 100 mM KPi (pH = 7.2) plus 150mM NaCl. Initial characterization of the degree of labeling (DOL) was conducted by UV/vis absorbance analysis, using a molar

DMD Fast Forward. Published on September 10, 2014 as DOI: 10.1124/dmd.114.060319
This article has not been copyedited and formatted. The final version may differ from this version.

extinction for the IR800 provided by the manufacture (ε_{777nm} = 270,000 in PBS : MeOH 1:1) and a correction factor of 0.03 to account for the contribution of the dye to absorbance at 280 nm. As a secondary confirmation of final protein concentration, the conjugate was subjected to IR analysis using a Direct Detect FTIR spectrometer (Millipore) to measure the characteristic amide-stretch frequency (1600-1700 cm^{-1}) previously calibrated with BSA standards. Final confirmation of the labeling was performed by LC/MS on an AB Sciex 5600 Triple TOF (Framingham, MA) coupled with a Shimadzu LC20 HPLC (San Alto, CA).

8C2 was radiolabeled with ^{125}I using a modified Chloramine- T method, as described in prior work (Garg and Balthasar, 2007). Briefly, 10 µL of Na-^{125}I (100 mCi/mL) was added to the antibody solution, and 20 µL of Chloramine-T (1 mg/mL in phosphate buffer) was then added to the mixture. The reaction was stopped after 90 s by the addition of 25 µL Na-metabisulfite (1 mg/mL in phosphate buffer), followed by 40 µL KI (10 mg/mL). Iodinated protein was purified by loading the reaction mixture unto a Sephadex G- 25 column (GE Healthcare, NJ). The purity of the iodinated IgG was assessed using instant thin layer chromatography (PE SiL-G, Whatman Ltd., Kent, England) (Garg and Balthasar, 2007). For all experiments, the purity of the iodinated preparation was higher than 99%.

8C2 Pharmacokinetics.

Male C57BL/6NHsd mice (Harlan Laboratories, Indianapolis, IN), age 6 to 9 weeks, weighing between 20 – 40 grams, were cared for in accordance to the *Guide for the Care and Use of Laboratory Animals, 8th* Edition (Michael B. Ballinger, 2011). All research protocols were approved by the Institutional Animal Care and Use Committee and studies were in compliance with the Animal Welfare Act Regulations (9 CFR3) and the guidelines published by the National Institutes of Health.

8C2 tissue distribution and plasma PK were studied in C57BL/6 mice (20-40g). To formulate the test article, unlabeled 8C2 and IR800-8C2 (DOL = 1.2) were mixed for a final average DOL of 0.2 and total 8C2 concentration of 1.4 mg/mL in PBS. The conjugate-containing mixture was dosed at 8 mg/kg intravenously via tail vein injection. Blood was collected from three animals per time point sacrificed by exsanguination at 1, 2, 6, 12, 24, 48, 96, 168, and 240 hr. After exsanguination, organs were harvested at each time point (liver, lung, GI, heart, kidney, bone, fat, muscle, skin, and spleen), rinsed with saline, blotted dry and weighed after which the tissues were frozen and stored at -70℃. Immediately prior to starting the homogenization procedure, the tissues were removed from the -70℃ freezer, weighed, and along with a 5 mm stainless steel grinding balls placed into a 96-well plate on ice. Chilled lysis buffer (50 mM Tris HCl, 100 mM NaCl, 0.1% Triton X-100, pH 7.4) containing a protease inhibitor cocktail (Roche, Indianapolis, Indiana) is then added at a volume equal to 2-fold the tissue mass (final conc. 1g tissue / 2 g buffer). The samples were homogenized using a Geno/Grinder 2010 (Metuchen, NJ).

IR800-8C2 conjugate levels were quantitated by fluorescence in both serum and tissue homogenates using the following generic assay: Briefly, standard curves (ranging from 7.5-0.001 µg/mL) were prepared with IR800-8C2 test article spiked in control tissue homogenate or serum diluted several fold to assess matrix effects on the linear fluorescence response. Fluorescence (Ex. = 784 nm, Em. = 800 nm) of each 20 µL sample was measured in 384-well small volume plate format with an Infinite M1000 Pro plate reader (Tecan). Separate QC samples were prepared to validate each curve. To quantify levels in tissues, the samples were diluted directly in PBS to match the tissue specific dilution matrix of each standard curve and quantified accordingly. The tissue concentrations were normalized to liver exposures for each individual animal. The final concentrations are reported in nM assuming a sample density of 1g/mL and an 8C2 MW = 150 kDa.

DMD Fast Forward. Published on September 10, 2014 as DOI: 10.1124/dmd.114.060319
This article has not been copyedited and formatted. The final version may differ from this version.

Plasma concentrations of 8C2 were also determined with the use of an antigen-capture enzyme-linked immunosorbent assay (ELISA). Briefly, 8C2 capture was performed with use of a cationized bovine serum albumin-topetecan conjugate (cBSA-top), synthesized through the use of a carbodiimide catalyzed amide bond reaction. Microplate (Nunc model # 62409-002, VWR, Bridgeport, NJ) wells were coated overnight with cBSA-top dissolved in pH 9, 0.02 mM Na_2HPO_4 (10 µg/ml, 250 µl/well). Plates were then washed with PB-Tween (0.05% Tween in 0.02 M Na2HPO4), followed by two washes of double-distilled water. Plates were then incubated with standards and samples in triplicate (200 µl) for 2 hrs at room temperature. At the end of incubation, the plates were washed and then incubated with 100 µl of goat anti-mouse-Fab alkaline phosphatase conjugate (Sigma, Cat #A1682, St. Louis, MO) for 1 h at room temperature (1:500 dilution of the conjugate with PB-Tween with 30% BSA). After washing, p-nitro phenyl phosphate solution (Pierce, Rockford, IL), 4 mg/ml in diethanolamine buffer, pH 9.8, was added to each well (250µl/well). The change in absorbance at 405 nm with respect to time (dA/dt) was measured (Spectra Max 340, Molecular Devices, Sunnyvale, CA), and standard curves were obtained by fitting dA/dt vs. 8C2 concentration.

The pharmacokinetics of ^{125}I-labeled 8C2 was conducted previously (Abuqayyas and Balthasar, 2012). Briefly, 8C2 was combined with a tracer dose of ^{125}I- 8C2 (10 µCi/mouse) and administered to a final dose of 8 mg/kg. Blood samples (20–40 µL) were collected from the retro-orbital plexus or from the sub-mandibular vein at 1, 3, 8, 24, 48, 96, 168 and 240 hours. Blood samples were centrifuged at 13,000 rpm for 5 min. Plasma fractions were collected and radioactivity was counted using a gamma counter (LKB Wallac 1272, Wallac, Turku, Finland). Radioactive counts were corrected for decay and background, and 8C2 plasma concentration was determined.

DMD Fast Forward. Published on September 10, 2014 as DOI: 10.1124/dmd.114.060319
This article has not been copyedited and formatted. The final version may differ from this version.

The catabolite of IR800-8C2, IR800-L-Lysine was formulated in 80% water and 20% DMSO to a total concentration of 2.0 mg/mL. The conjugate-containing mixture was dosed at 1 mg/kg intravenously via tail vein injection. Blood was collected from animals via retro-orbital sinus punctures for each time point; at 0, 0.25, 0.5, 1, 3, 5 and 8hr time points. Blood was transferred into Microtainer Brand Tube. Twenty minutes at room temperature was allowed for clot formation to generate ~50 µL of serum. 1/50 dilutions were carried out into PBS (pH 7.4) and analyzed for fluorescence (Ex. = 784 nm, Em. = 800 nm) in 384-well small volume plates with an Infinite M1000 Pro plate reader (Tecan) as described for IR800-8C2 above.

Whole Body Imaging.

A subset of animals (N = 9) dosed with IR800-8C2 and a separate subset (N = 3) dosed with vehicle only were reserved for whole body sectioning. Briefly, mice previously sacrificed and exsanguinated were frozen in a hexane/dry ice bath for approximately 2 min. The carcasses were then drained and blotted dry before storage on dry ice for at least 2 hrs. The frozen carcasses were transferred to a bed of carboxymethylcellulose and frozen into blocks. Whole-body saggital sections were generated using a Leica CM3600 cryomicrotome, and 40 micron thick sections were mounted and sealed between two layers of non-fluorescent adhesive tape.

Fluorescence imaging of the saggital sections was conducted using an Odyssey CL_x infrared imager (LI-COR). Briefly, a saggital section was fixed directly to the surface of the imager and the minimum scanning field defined in Image Studio software (v2.1, LI-COR). The following settings were defined prior to data acquisition using the designated 800 channel: resolution (µ) = 42 µm, Quality (Q) = High, focus offset (f) = 0.0 mm, Intensity = 40. Whole body slices were used for qualitative and quantitative analysis. For quantitative analysis, the organs of interest were manually outlined and the fluorescence intensity over the area of each region of interest

DMD Fast Forward. Published on September 10, 2014 as DOI: 10.1124/dmd.114.060319
This article has not been copyedited and formatted. The final version may differ from this version.

was integrated and normalized to the signal measured in liver using Image Studio (LI-COR, Lincoln, NE).

Non-compartmental Pharmacokinetic Data Analysis.

The mean area under the plasma or tissue concentration–time curves (AUC 0–10 days) were calculated for each measurement technique employed to assay 8C2 using the NCA in WinNonlin 6.1 (Phoenix, Pharsight Corporation, Palo Alto, CA). Plasma clearance (CLp) and volume of distribution at steady-state (Vss) were also determined using NCA.

Results

8C2 Antibody Labeling and Characterization.

Based upon the sensitivity of the IR800 dye and the desire to minimize potential effects of labeling on the antibody physicochemical properties, a low dye to protein ratio was targeted to achieve an average stoichiometry near 1:1. The resultant labeled antibody was characterized by UV and LC-MS to determine the dye to antibody stoichiometry and were in good agreement, with estimates of 1.2 and 1.4 moles of dye to antibody by UV and MS, respectively (data not shown). Removal of unreacted dye was achieved via buffer exchange and confirmed by SEC. Analytical SEC of the IR800 conjugate mixture showed that the antibody was retained predominantly as a monomer and had < 5% IR800 dye remaining (Figure 1).

8C2 Pharmacokinetics.

8C2 antibody serum exposures were determined directly by fluorescence based upon IR800 dye optical properties and by ELISA (Figure 2). The pharmacokinetic parameters were determined by NCA as described in the methods section and are shown in Table 1. The initial concentrations (C_0) were similar at 672 and 624 nM, when measured directly with fluorescence and ELISA detection, respectively. The clearance derived from the two methods was estimated at 8.4 mL/day/kg with direct fluorescence compared to 2.5 mL/day/kg for the ELISA method.

DMD Fast Forward. Published on September 10, 2014 as DOI: 10.1124/dmd.114.060319
This article has not been copyedited and formatted. The final version may differ from this version.

The disparity in clearance resulted in a 42% decrease in total exposure when measured by IR800 directly. The AUC was correspondingly 1.9-fold lower for the IR800 labeled material. TCA treated serum resulted in no detectable fluorescent signal. The pharmacokinetic parameters by ELISA were similar to those measured previously by ^{125}I-labeled 8C2 directly (Abuqayyas and Balthasar, 2012).

Tissue Quantitation with IR800-8C2 and ^{125}I-8C2.

8C2 tissue concentrations were evaluated by fluorescence detection in the liver, spleen, heart, lung, GI, kidney, muscle, skin and bone. The area under the curve (AUC) for each tissue was calculated using non-compartmental analysis. The parameters are reported in (Table 2). Previously, tissue distribution for ^{125}I-labeled 8C2 was reported (Abuqayyas and Balthasar, 2012), and these results are also included in Table 2. A comparison of IR800-8C2 and ^{125}I-8C2 tissue pharmacokinetic profiles is captured in Figure 3. Comparative analysis revealed consistently decreased exposure for the IR800-8C2 mAb compared to ^{125}I-8C2. On average most tissues had 35% lower exposure compared to tissues measured with ^{125}I-8C2 (excluding the liver). In contrast, the liver exhibited a 3.8-fold increase C_{max} for IR800-8C2 relative to ^{125}I-8C2, at 409 nM ± 36 nM versus 108 nM ± 20 nM, respectively. The corresponding AUC_{0-10} was 32% greater in the liver for IR800-8C2 compared to ^{125}I-8C2. The kidney, lung and spleen all had similar initial concentrations between the two tracers. For example, the kidneys showed similar initial tissue concentration of 164 nM ± 34 nM for IR800-8C2 compared to 139 nM ± 16 nM for ^{125}I-8C2, but then the IR800-8C2 concentrations fell sharply after 24 hours leading to an overall 3.9 fold lower tissue AUC_{0-10}. A similar trend was observed for lung and spleen (Figure 2). All other tissues measured using IR800-8C2 showed substantial decrease in exposures relative to ^{125}I-8C2 ranging from 10% to 33% of the AUC_{0-10}, respectively (Table 2). Upon correcting for exposures of 8C2 in the blood compartment, the tissue exposures for IR800-8C2 were not substantially increased except for the liver (Figure 5).

Whole body cross-sectioning with IR800-8C2.

Whole body cross-sections (WBS, sagittal plane) were taken at specific time points to capture tissue exposures and for comparison to quantitative organ homogenization. Representative images are displayed in Figure 4. In total, five levels were taken with level 1 being the outermost cross-section (closest to the skin) and level five representing cross-section closest to the midline of the animal (Figure 4A). A representative time course at level 2 is shown in Figure 4B and provides a time course of exposure to the major organs. At the initial time point it was evident IR800-8C2 was well distributed. In specific, the liver and bone marrow retained high levels of mAb. Organs of interest were quantified using LI-COR software (Image Studio v2.1). An attempt to use the whole body cross-sections to semi-quantitatively measure tissue exposure was made by delineating the individual organs in the software prior to measurement of the integrated fluorescence intensity that was then normalized against that of the liver. A comparison of the whole body sections to the homogenized organs is shown in Figure 5. The kidney, heart, muscle, bone and GI were evaluated. In all tissues except the GI the levels determined from WBS were lower than those derived directly from tissue homogenization. However, there were no statistically significant differences observed between the two methods.

DMD Fast Forward. Published on September 10, 2014 as DOI: 10.1124/dmd.114.060319
This article has not been copyedited and formatted. The final version may differ from this version.

Discussion

The differential serum exposure observed upon dosing IR800-8C2 depending on the quantitation assay employed (ELISA or direct IR800 fluorescence) was unexpected. Previous work (Oliveira et al., 2012) highlights the utility of the IR800 dye attached to antibodies as a method for evaluating mAb biodistribution. In that study, the authors employed a dual labeling approach wherein cetuximab was labeled with desferal-chelated positron emitter zirconium (^{89}Zr) and IR800 on the same mAb molecule to yield ^{89}Zr-cetuximab-IR800 (Oliveira et al., 2012).This approach yielded similar patterns in biodisposition of the two tracers. Unfortunately, the comparison of dual labeled ^{89}Zr-cetuximab-IR800 to ^{89}Zr-cetuximab rather than to unlabeled cetuximab confounds any interpretation of changes in drug disposition induced independently by either tracer.

Previously, Cohen et al. had highlighted the limitations of IR800 with regard to altered liver uptake, yet that study also drew conclusions from the use of mAb containing both desferal-^{89}Zr and IR800 tracers (Cohen et al., 2011). The results reported therein describe increased liver uptake when IR800 dye to mAb levels exceeded >1.5. With these previous results in mind, our aim was to keep the degree of labeling ≤ 1.5 in order to minimize the potential impact of IR800 on pharmacokinetics. However, even with these precautions, an effect was observed with respect to IR800-8C2 serum exposure. It is plausible that the differences in physicochemical properties of the 8C2 and cetuximab antibodies contribute to their unique biodistribution. Alternatively, the rather moderate alteration in blood clearance and biodistribution into tissues observed by Cohen et al. when using 1-2 molecules of IR800 may have been influenced by the co-conjugation of the desferyl chelate moiety which may have masked some of the effects of IR800 tracer in the case of ^{89}Zr-cetuximab-IR800.

Previously, our lab has evaluated the IR800 dye to characterize biodistribution for several therapeutic proteins and mAbs. For example, a 55 kDa mAb fragment bearing the IR800

DMD Fast Forward. Published on September 10, 2014 as DOI: 10.1124/dmd.114.060319
This article has not been copyedited and formatted. The final version may differ from this version.

dye as the tracer displayed a PK profile indistinguishable from the unlabeled molecule (Supplemental Figure 1a). An important distinction between this fragment and IR800-8C2 mAb is that it has much faster clearance compared to a full mAb (hrs vs. days). One possibility for the apparent lack of IR800 label-related effects during our previous study is that the molecule exhibits an inherently high clearance and short $t_{1/2}$ that could mitigate any impact of IR800 tracer on the PK. Thus, we hypothesize that low clearance and long mean residence time are requisites to observe deviations in clearance from the parent molecule (i.e. the stark IR800-dependent increase in CL will be sufficiently resolved). In support of our hypothesis, we have since examined other IR800-labeled mAbs and have observed similar results to those reported herein (Supplemental Figure 1b). These observations suggest that the effects of IR800 protein disposition are not mAb-specific, which may markedly limit the utility of this probe for quantitative tissue biodistribution studies, at least for mAb-based therapeutics. Work in our lab is ongoing to test whether the short half-lives of IR800-labeled mAb fragments, such as Fab and $F(ab)_2$, mask the effects of IR800 on the observed pharmacokinetics and tissue distribution.

A benefit of using mouse mAb 8C2 as a model IgG1 is the lack of endogenous antigen, and it therefore displays linear pharmacokinetics, as previously demonstrated (Abuqayyas and Balthasar, 2012). Importantly, these properties facilitate the comparison to previously reported PK studies of 8C2 with ^{125}I as the labeling agent. The pharmacokinetic parameters observed with IR800-8C2 were distinct from the ^{125}I-8C2 data when measured using IR800 fluorescence. However, when the IR800-8C2 was measured by ELISA the data were comparable to those determined previously by gamma counting via the attached ^{125}I label (Figure 2). The distinction in analytical methods is that IR800 fluorescent detection measures only the conjugated 8C2 whereas the ELISA measures both the conjugated and unconjugated mAb. As such, the different results could arise via several mechanisms. The IR800 label on the mAb could be unstable yielding unreliable quantitation by fluorescence. *In vitro* incubations in plasma over 48

hours did not produce any loss in fluorescent signal (data not shown). In addition, analysis of TCA-precipitated serum supernatant revealed no fluorescent signal (<1 ng/mL) implying that IR800-8C2 circulates intact, and is consistent with previous stability experiments (Oliveira et al., 2012). Fluorescence quenching is another possible rationale for a discrepancy in PK parameters, but the sensitivity of IR800 allowed for rather large dilutions that minimize this risk. Furthermore, if quenching was to occur, one would expect this effect to be variable across different tissues and this is inconsistent with the tissue PK that exhibits similar elimination rates for all sample types.

To further investigate if tissue specific uptake was responsible for the accelerated clearance of IR800-8C2, quantitative tissue analysis was performed. The ^{125}I-8C2 tissue distribution data previously generated was used as a baseline of what might be expected for IR800-8C2 (Figure 3). The liver showed higher 8C2 concentrations for the first 5 days with the IR800 tracer versus ^{125}I-8C2. Given that the liver is one of the primary clearance organs for mAbs, this increase is likely responsible for the lower serum exposures of IR800-8C2. It is important to recognize that the higher concentrations of IR800-8C2 could also be related to the residualizing nature of the IR800 tracer compared to ^{125}I. However, upon analysis of the other tissues the IR800 levels were consistently lower than those obtained with ^{125}I. These findings are at odds with what would be expected for a residualizing tracer that is anticipated to have greater tissue exposure relative to a non-residualizing ^{125}I (Table 2; Ratio of IR800 T:S/^{125}I T:B). Therefore, the increased liver concentrations for IR800-8C2 do not appear to be a result of differences in residualizing properties between the two tracers. The increased liver signal is most likely due to increased specific uptake and elimination of IR800-8C2. Previous studies demonstrated specific uptake of several proteins, including IgG, into mouse liver nonparenchymal cells via scavenger receptors after modification with succinic acid to alter the negative charge density (Yamasaki et al., 2002). By extension, it is possible that conjugation of

DMD Fast Forward. Published on September 10, 2014 as DOI: 10.1124/dmd.114.060319
This article has not been copyedited and formatted. The final version may differ from this version.

IgG with IR800, which bears several sulfonic acid groups, may influence the disposition of IR800-8C2 in a similar fashion.

Previously, parallels between IR800 tissue concentrations to those observed with ^{89}Zr provide evidence (Oliveira et al., 2012) to support that IR800 can behave as a residualizing tracer. However, as mentioned previously, that study evaluated a dual labeled (^{89}Zr and IR800) molecule. It is plausible that the dual labeling approach interferes with the inherent properties of the IR800. Specifically, the ^{89}Zr chelate desferyl moiety could impact the cellular disposition of the IR800 catabolite. We have identified the major catabolite from IR800 protein conjugation to be IR800-L-lysine (data not shown). Therefore, in a separate mouse study, we administered an IV dose of IR800-L-lysine and observed rapid clearance from serum (Figure 2). The rapid elimination of IR800-L-lysine ($t_{1/2}$ < 1hour) is consistent with the molecules zwitterionic character that should lead to low permeability. To this end, the formation of the IR800-L-lysine in the cell upon catabolism of IR800-8C2 could lead to reduced cellular efflux. These findings support further investigation into the tracer properties of IR800.

Lastly, an additional aim of this work was to evaluate the ability of IR800 tracer in combination with whole body imaging using a fluorescent scanner as an affordable, rapid method to perform tissue biodistribution studies. The technique is capable of generating quality images using a basic laboratory infrared scanner and can be used to detect exposures to the major organs (Figure 4), similar to QWBA techniques. Ideally, the whole body imaging could represent the tissue concentrations that were determined by homogenization. Figure 5 compares the tissue homogenized AUC_{0-10} values compared to the organ quantified by ROI at the 48 h time point, demonstrating the feasibility of this approach. The tissue levels were normalized to the liver values determined from each analytical technique. The two methods did not yield any statistical difference in the subset of tissue analyzed illustrating the potential value of this approach. Several advantages of this technique are the ability to rapidly sample across

the entire organ in addition to specific regions of interest. This method also allows strict boundaries to be drawn between tissues. One drawback is that not all organs are clearly identifiable within the cross sections. Further optimization of the technique should be employed in an attempt to improve the translation of data from whole body imaging to that from homogenization using a fluorescent tracer that does not impact protein disposition. For example, it is possible to vary the chosen tissue slice thickness, and this may allow less heterogeneous tissue sampling in a thicker slice; alternatively, one could aim for less variability in fluorescent signal via signal quenching if the slice thickness is reduced.

Based upon the findings herein, the IR800 as a tracer for proteins clearly impacts the pharmacokinetics of mAbs and is not ideal for determining absolute tissue distribution in mice. However, the sensitivity and selectivity of the IR800 tracer is obvious and the potential to provide exquisite contrast from background enables clear distinction of antigen expressing tissues in mouse xenograft models and can serve as a useful tracer for intra-operative imaging (Kovar et al., 2009; Keereweer et al., 2012). Investigations into the mechanism(s) leading to the accelerated serum PK and enhanced liver uptake are ongoing. Defining the translation of these findings from the mouse to humans will be important to developing quantitative optical imaging techniques and can provide additional characterization for use of fluorescent tracers as clinical diagnostic tools.

Authorship Contributions

Participated in research design: Conner, Wienkers, Abaquayyas, D.Rock

Conducted experiments: Conner, B.Rock, Kwon, D.Rock

Contributed new reagents or analytic tools: Balthasar

Performed data analysis: Conner, D.Rock

Wrote or contributed to the writing of the manuscript: Conner, B.Rock, D.Rock

References

Abuqayyas L and Balthasar JP (2012) Application of knockout mouse models to investigate the influence of FcgammaR on the tissue distribution and elimination of 8C2, a murine IgG1 monoclonal antibody. *International journal of pharmaceutics* **439:**8-16.

Aerts HJ, Dubois L, Perk L, Vermaelen P, van Dongen GA, Wouters BG, and Lambin P (2009) Disparity between in vivo EGFR expression and 89Zr-labeled cetuximab uptake assessed with PET. *Journal of nuclear medicine : official publication, Society of Nuclear Medicine* **50:**123-131.

Boswell CA, Mundo EE, Firestein R, Zhang C, Mao W, Gill H, Young C, Ljumanovic N, Stainton S, Ulufatu S, Fourie A, Kozak KR, Fuji R, Polakis P, Khawli LA, and Lin K (2013) An integrated approach to identify normal tissue expression of targets for antibody-drug conjugates: case study of TENB2. *British journal of pharmacology* **168:**445-457.

Boswell CA, Tesar DB, Mukhyala K, Theil FP, Fielder PJ, and Khawli LA (2010) Effects of charge on antibody tissue distribution and pharmacokinetics. *Bioconjug Chem* **21:**2153-2163. doi: 2110.1021/bc100261d. Epub 102010 Nov 100265.

Chen J, Lu Q, and Balthasar JP (2007) Mathematical modeling of topotecan pharmacokinetics and toxicodynamics in mice. *Journal of pharmacokinetics and pharmacodynamics* **34:**829-847.

Cohen R, Stammes MA, de Roos IH, Stigter-van Walsum M, Visser GW, and van Dongen GA (2011) Inert coupling of IRDye800CW to monoclonal antibodies for clinical optical imaging of tumor targets. *EJNMMI Res* **1:**31. doi: 10.1186/2191-1219X-1181-1131.

Duncan JR and Welch MJ (1993) Intracellular metabolism of indium-111-DTPA-labeled receptor targeted proteins. *J Nucl Med* **34:**1728-1738.

Fast JL, Cordes AA, Carpenter JF, and Randolph TW (2009) Physical instability of a therapeutic Fc fusion protein: domain contributions to conformational and colloidal stability. *Biochemistry* **48:**11724-11736.

Garg A and Balthasar JP (2007) Physiologically-based pharmacokinetic (PBPK) model to predict IgG tissue kinetics in wild-type and FcRn-knockout mice. *Journal of pharmacokinetics and pharmacodynamics* **34:**687-709.

Geissler F, Anderson SK, and Press O (1991) Intracellular catabolism of radiolabeled anti-CD3 antibodies by leukemic T cells. *Cell Immunol* **137:**96-110.

Guo W, Zhang L, Ji J, Gao W, Liu J, and Tong M (2014) Breast cancer sentinel lymph node mapping using near-infrared guided indocyanine green in comparison with blue dye. *Tumour biology : the journal of the International Society for Oncodevelopmental Biology and Medicine* **35:**3073-3078.

Herzog E, Harris S, Henson C, McEwen A, Schenk S, Nolte MW, Pragst I, Dickneite G, Schulte S, and Zollner S (2014) Biodistribution of the recombinant fusion protein linking coagulation factor IX with albumin (rIX-FP) in rats. *Thromb Res* **133:**900-907. doi: 910.1016/j.thromres.2014.1002.1010. Epub 2014 Feb 1022.

Keereweer S, Kerrebijn JD, Mol IM, Mieog JS, Van Driel PB, Baatenburg de Jong RJ, Vahrmeijer AL, and Lowik CW (2012) Optical imaging of oral squamous cell carcinoma and cervical lymph node metastasis. *Head & neck* **34:**1002-1008.

Korth-Bradley JM, Rubin AS, Hanna RK, Simcoe DK, and Lebsack ME (2000) The pharmacokinetics of etanercept in healthy volunteers. *The Annals of pharmacotherapy* **34:**161-164.

Kovar JL, Volcheck W, Sevick-Muraca E, Simpson MA, and Olive DM (2009) Characterization and performance of a near-infrared 2-deoxyglucose optical imaging agent for mouse cancer models. *Analytical biochemistry* **384:**254-262.

Lee SB, Hassan M, Fisher R, Chertov O, Chernomordik V, Kramer-Marek G, Gandjbakhche A, and Capala J (2008) Imaging epidermal growth factor receptor expression in vivo: pharmacokinetic and

biodistribution characterization of a bioconjugated quantum dot nanoprobe. *Clin Cancer Res* **14:**3840-3849. doi: 3810.1158/1078-0432.CCR-3807-4076.

Michael B. Ballinger PJRB, Stephen W. Barthold, Linda C. Cork, Jann Hau, Michael J. Huerkamp, Michael D. Kastello, Arthur L. Lage, Christian Lawrence, Randall J. Nelson, Steven M. Niemi, Melinda A. Novak (2011) Guide for the Care and Use of Laboratory Animals, 8th Edition (ACADEMES TNRCOTN ed, pp 1-246, The National Academy Press, Washington, D.C.

Oliveira S, Cohen R, Walsum MS, van Dongen GA, Elias SG, van Diest PJ, Mali W, and van Bergen En Henegouwen PM (2012) A novel method to quantify IRDye800CW fluorescent antibody probes ex vivo in tissue distribution studies. *EJNMMI Res* **2:**50. doi: 10.1186/2191-1219X-1182-1150.

Perera RM, Zoncu R, Johns TG, Pypaert M, Lee FT, Mellman I, Old LJ, Toomre DK, and Scott AM (2007) Internalization, intracellular trafficking, and biodistribution of monoclonal antibody 806: a novel anti-epidermal growth factor receptor antibody. *Neoplasia* **9:**1099-1110.

Sands H (1990) Experimental studies of radioimmunodetection of cancer: an overview. *Cancer Res* **50:**809s-813s.

Steiner M, Gutbrodt K, Krall N, and Neri D (2013) Tumor-targeting antibody-anticalin fusion proteins for in vivo pretargeting applications. *Bioconjugate chemistry* **24:**234-241.

Tanaka E, Ohnishi S, Laurence RG, Choi HS, Humblet V, and Frangioni JV (2007) Real-time intraoperative ureteral guidance using invisible near-infrared fluorescence. *The Journal of urology* **178:**2197-2202.

Yamasaki Y, Sumimoto K, Nishikawa M, Yamashita F, Yamaoka K, Hashida M, and Takakura Y (2002) Pharmacokinetic analysis of in vivo disposition of succinylated proteins targeted to liver nonparenchymal cells via scavenger receptors: importance of molecular size and negative charge density for in vivo recognition by receptors. *The Journal of pharmacology and experimental therapeutics* **301:**467-477.

Yip V, Palma E, Tesar DB, Mundo EE, Bumbaca D, Torres EK, Reyes NA, Shen BQ, Fielder PJ, Prabhu S, Khawli LA, and Boswell CA (2014) Quantitative cumulative biodistribution of antibodies in mice: Effect of modulating binding affinity to the neonatal Fc receptor. *MAbs* **6:**689-696. doi: 610.4161/mabs.28254. Epub 22014 Feb 28226.

Zhu H, Baxter LT, and Jain RK (1997) Potential and limitations of radioimmunodetection and radioimmunotherapy with monoclonal antibodies. *J Nucl Med* **38:**731-741.

Figure Legends

Figure 1. SEC/UV Characterization of 8C2 mAb (a), IR800 (b) and IR800-8C2 mAb (c). SEC chromatograms of both (a) and (c) were acquired after injection of 35 µg of protein material; a 20µL injection of 5uM IR800 dye solution was used for collection of (b). Note: the data for the 780nm channel in (c) were multiplied by a factor of 2.

Figure 2. Serum Pharmacokinetics of 8C2 by ELISA and with direct fluorescence of the conjugate compared to ^{125}I-8C2. Additional pharmacokinetic profiles include TCA precipitated serum samples and catabolite, IR800-L-Lysine.

Figure 3. Tissue pharmacokinetic profiles for IR800-8C2 and ^{125}I-8C2

Figure 4. Whole body cross-sectional Imaging of IR800-8C2 highlighting the different depths of saggital sectioning to highlight different anatomy: skin (1), eye (2), kidney (3), lung (4), liver (5), spine (6), brain (7), heart (8) and GI (9). Time course of IR800-8C2 tissue exposures (2, 48 and 240 h) and vehicle control (C) with whole body slices (N=3 animals per time point).

Figure 5. Comparison of semi-quantitation of cross-sectional tissue images to tissue homogenates of IR800-8C2 at 48 hours. Each tissue analysis represents tissues from 3 individual animals. The errors bars represent standard deviation. Statistical differences across techniques was evaluated by t-Test with p-values for each tissue are in parenthesis; kidney (0.62), heart (0.79), muscle (0.08), bone (0.14), GI (0.72).

DMD Fast Forward. Published on September 10, 2014 as DOI: 10.1124/dmd.114.060319
This article has not been copyedited and formatted. The final version may differ from this version.

Table 1. Pharmacokinetic Analysis of 8C2 labeled antibody. IR800-8C2 was measured by ELISA or Fluorescence from the IR800. The i125 was measured directly by gamma counter. ^The pharmacokinetics of the catabolite of the IR800-8C2, Lys-IR800 was also characterized. Pharmacokinetics were assessed with N=3 animals per group. Standard deviations are indicated in parenthesis.

Test Article	Analytical Technique	AUC (nM*day)	CL (mL/d/kg)	Vdss (mL/kg)	C_0 (nM)	T1/2 (day)
IR800-8C2	ELISA	1628 (68)	2.5 (0.2)	30 (1)	624 (142)	7.4 (0.8)
	Fluorescence	875 (115)	8.4 (1.1)	33 (4)	672 (81)	2.7 (0.3)
^{125}I-8C2	Gamma count	2145 (51)	1.8 (0.2)	26 (2)	638 (61)	10.1 (3.1)
Lysine-IR800^	Fluorescence	104 (27)	21.3 (4.1)	592 (8)	2027 (289)	0.05 (0.01)

^Dosed separately; Lys-IR800 is the major protein catabolite of NHS-IR800 labeled proteins. Parameters are derived from triplicate measurements with average and (standard deviation) reported.

DMD Fast Forward. Published on September 10, 2014 as DOI: 10.1124/dmd.114.060319
This article has not been copyedited and formatted. The final version may differ from this version.

Table 2. Tissue Exposure of IR800-8C2 Compared to 125I-8C2.

Tissue	AUC (IR800)[1] nM*day	AUC (^{125}I) nM*day	AUC (IR800): AUC (^{125}I)	TB (IR800): TB (^{125}I)[2]
Liver	636.1 (69)	483.7 (57.1)	1.32	3.24
Spleen	117.1 (15.5)	560.5 (56.9)	0.21	0.52
Lung	213.6 (13.9)	656.4 (65.1)	0.33	0.80
Heart	41.0 (6.6)	406.8 (33.3)	0.10	0.25
Kidney	130.1 (23)	505.5 (45.6)	0.26	0.63
Skin	80.1 (0.5)	630.8 (27.8)	0.13	0.31
Muscle	21.3 (1.4)	1889.9 (7.9)	0.11	0.28
Bone	61.2 (3.3)	324.9 (15.2)	0.19	0.46
GI	56.2 (3.1)	350.3 (101.3)	0.16	0.39

[1]AUC determined directly by IR800 fluorescence. [2] TB represents the tissue to blood ratio. Parameters are derived from triplicate measurements with average and (standard deviation) reported.

Figure 1

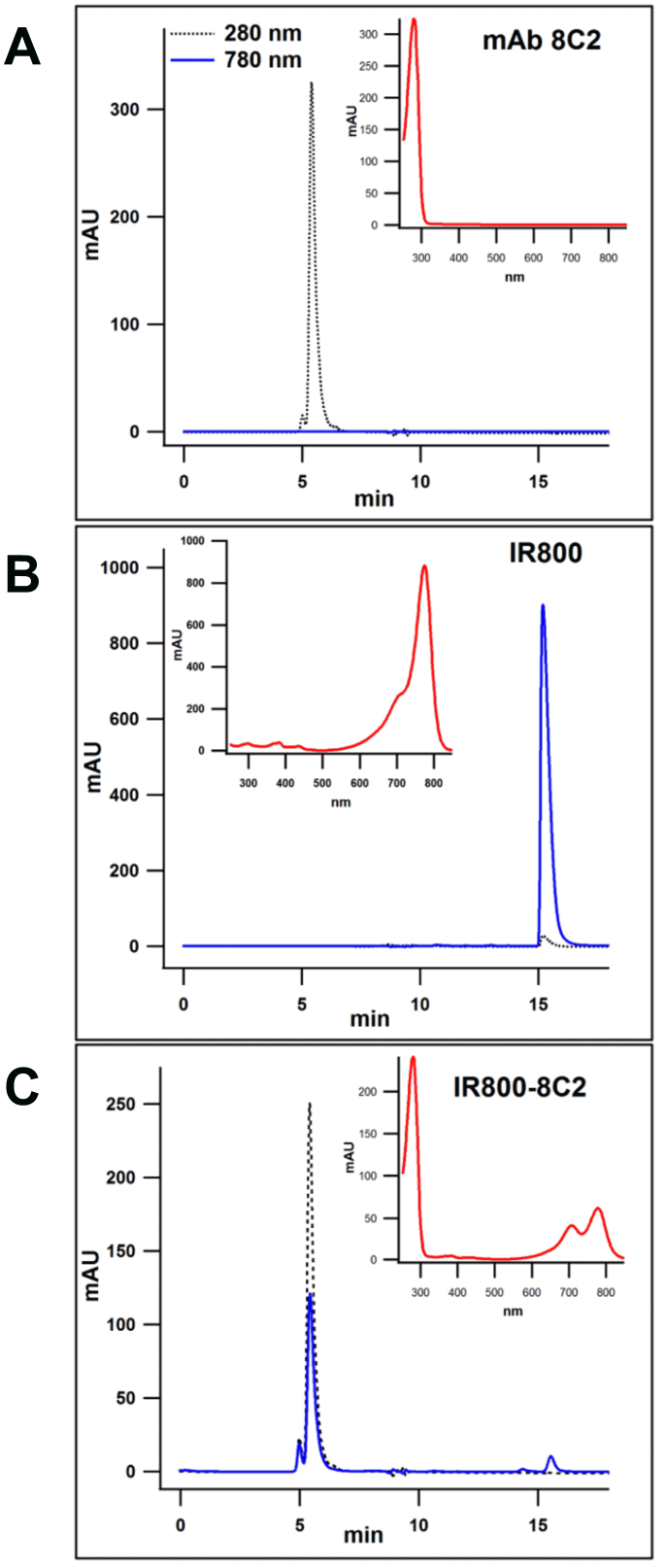
A
280 nm
780 nm
mAb 8C2
mAU
min
nm
B
IR800
mAU
min
nm
C
IR800-8C2
mAU
min
nm

Figure 2

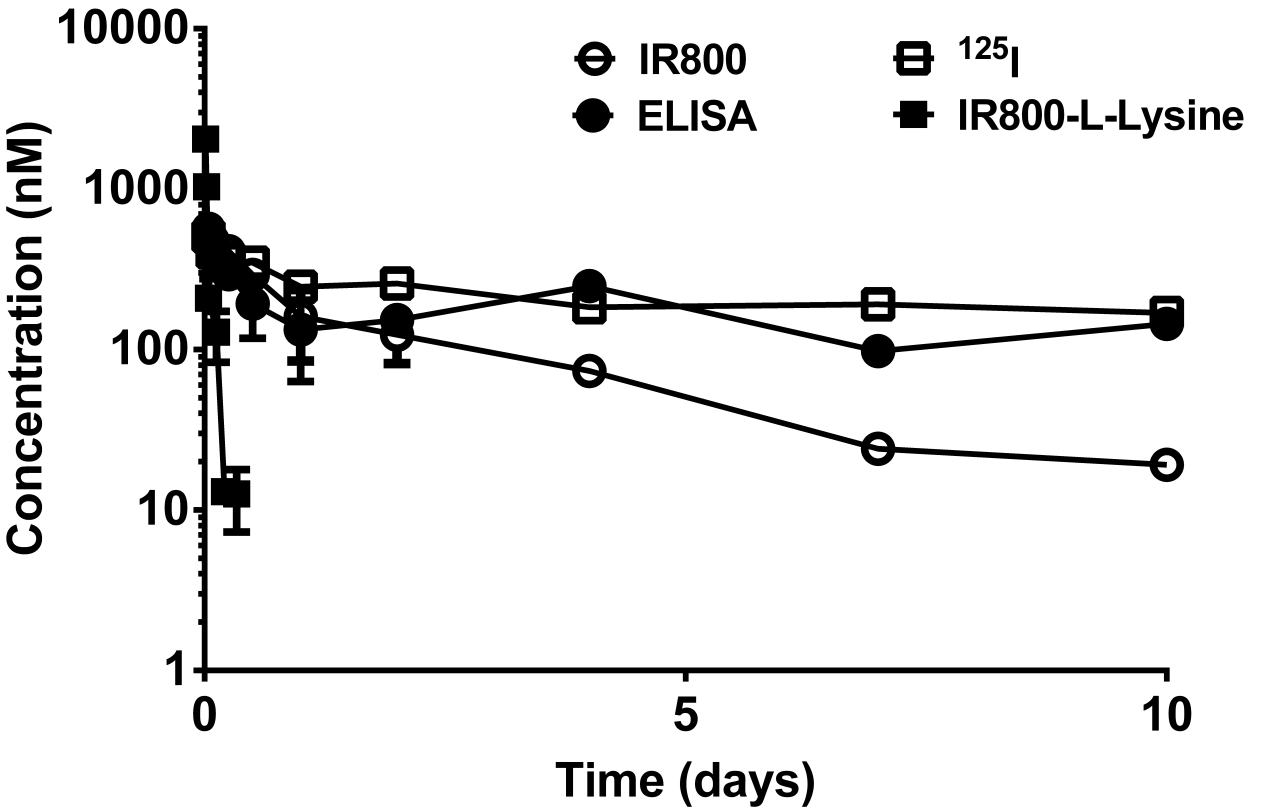
10000
1000
100
10
1
Concentration (nM)
0
5
10
Time (days)
IR800
ELISA
125I
IR800-L-Lysine

Figure 3

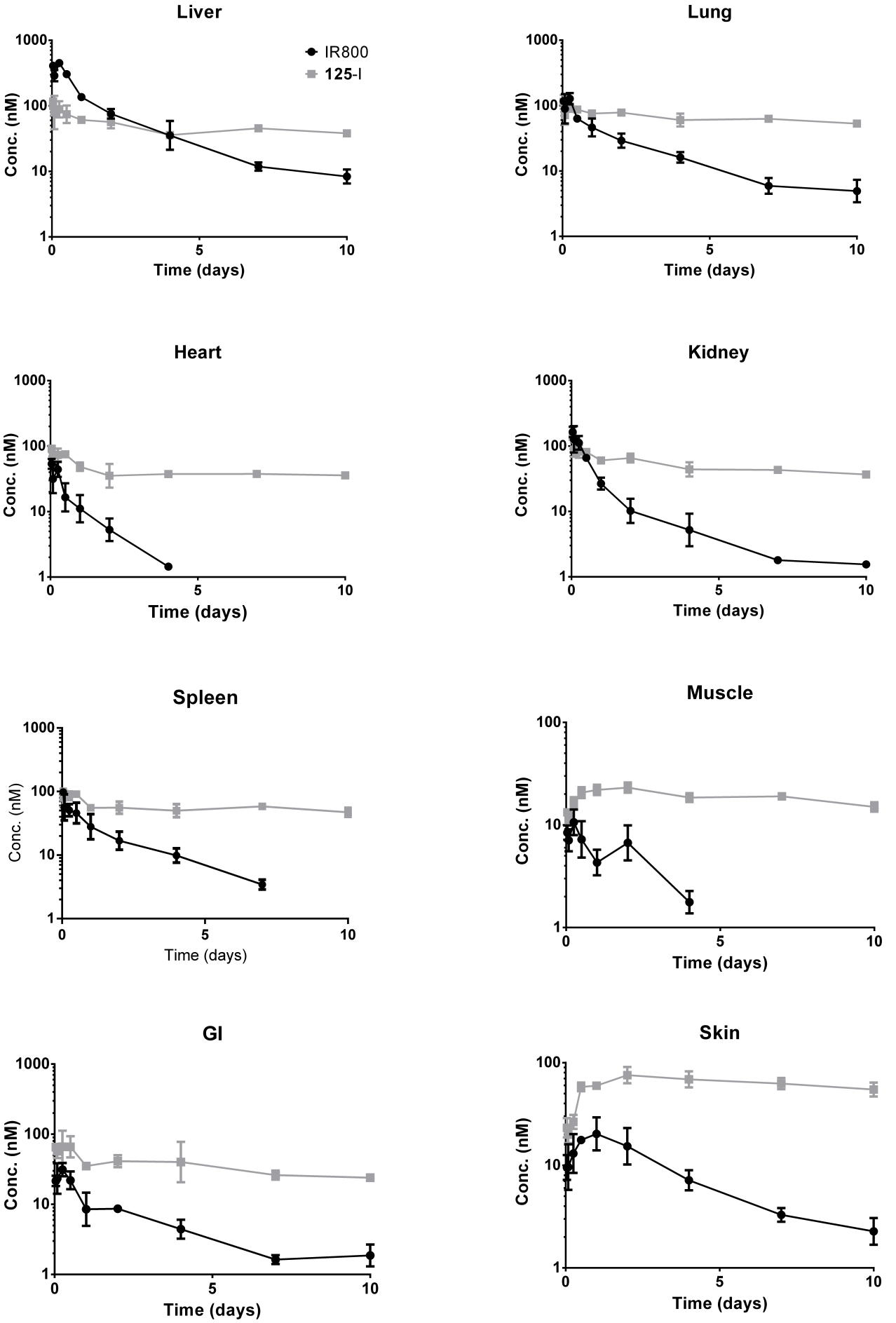
Liver
IR800
125-I
Conc. (nM)
Time (days)
Lung
Heart
Kidney
Spleen
Muscle
GI
Skin

Figure 4

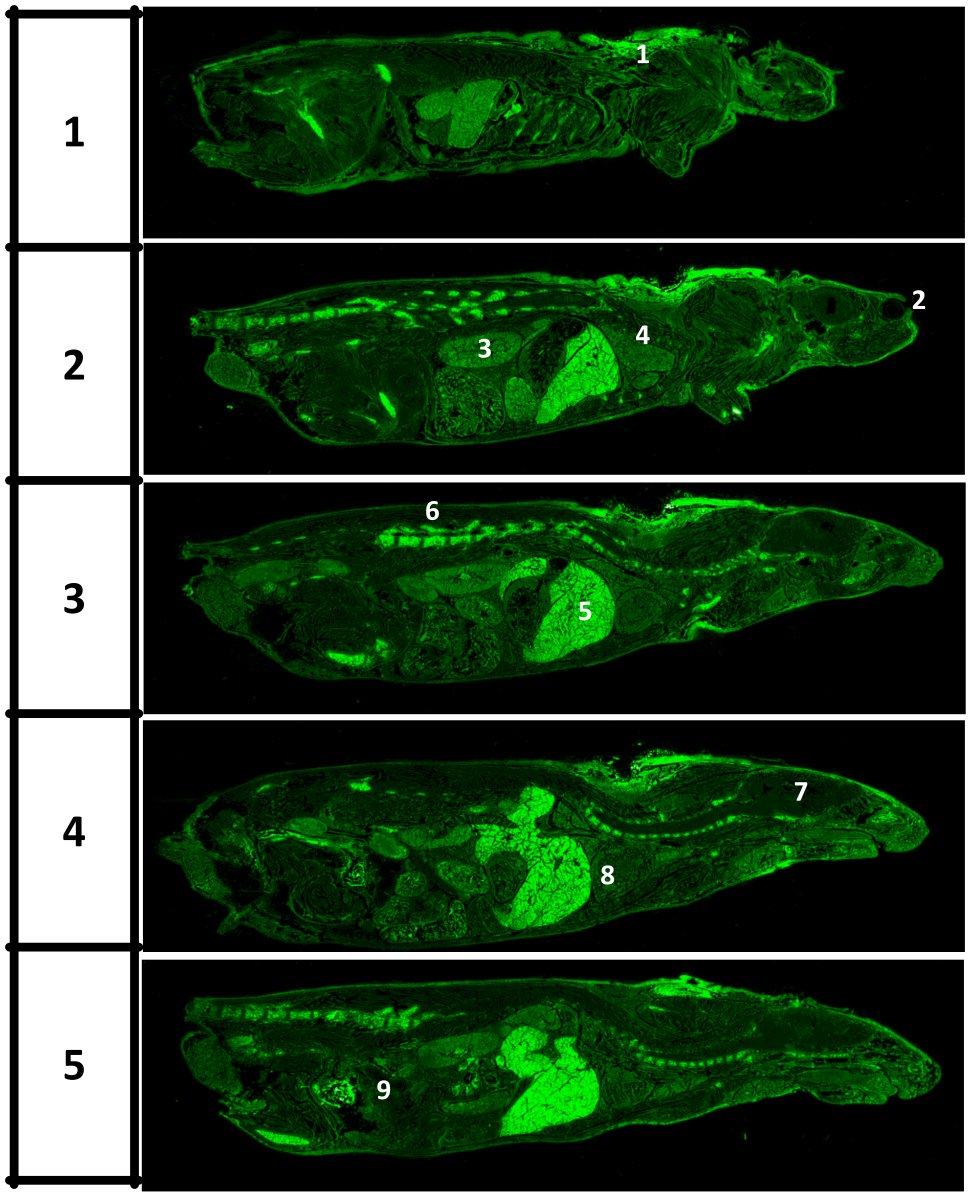

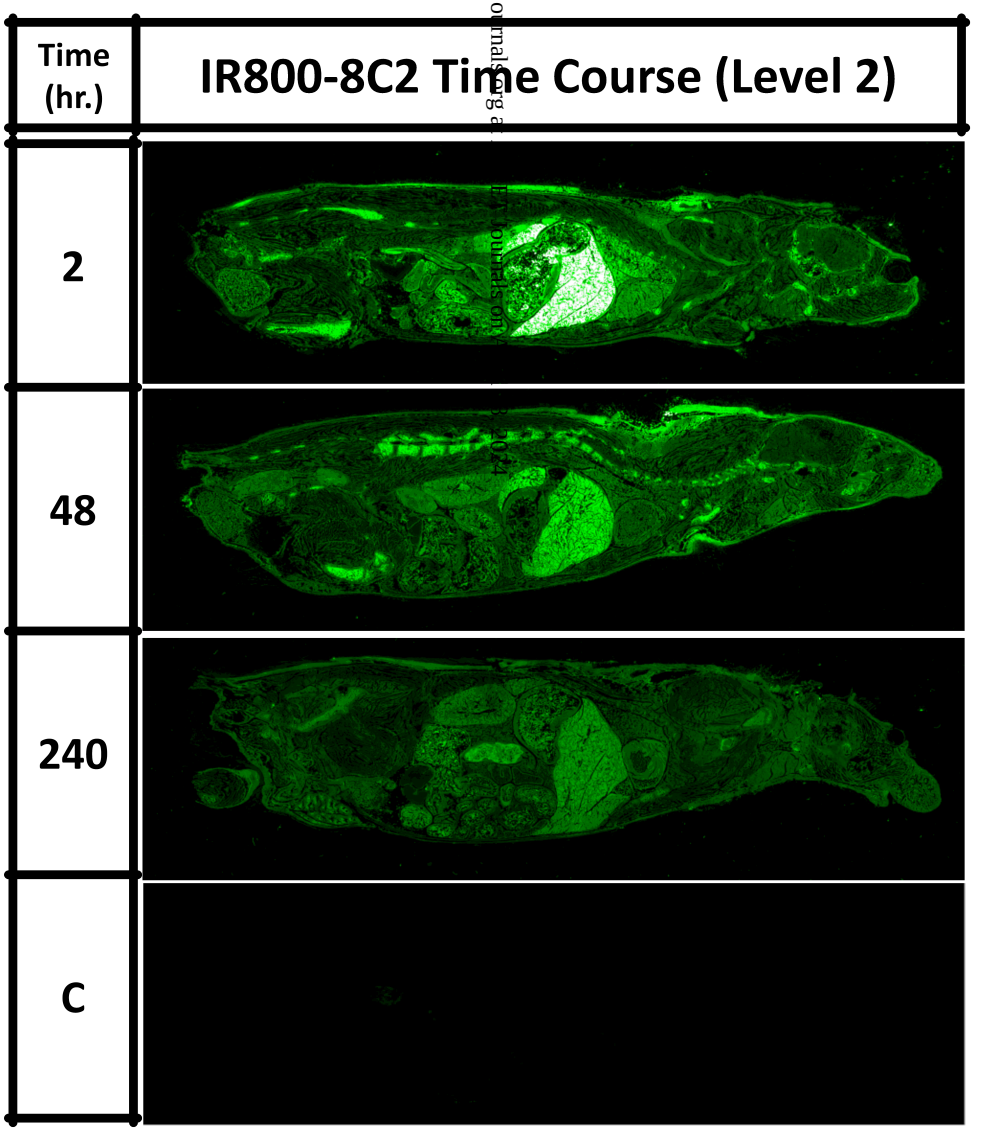

Figure 5